ELSEVIER

18 July 1997

Chemical Physics Letters 273 (1997) 107–114

CHEMICAL PHYSICS LETTERS

A global potential energy surface for the H_3^+ molecule

Rita Prosmiti, Oleg L. Polyansky [1], Jonathan Tennyson

Department of Physics and Astronomy, University College London, Gower St., London WC1E 6BT, UK

Received 14 April 1997; in final form 19 May 1997

Abstract

A global two-valued ground-state potential for H_3^+ is constructed. The energy switching approach is used to combine different functional forms for three different energy regimes. The Born–Oppenheimer surface of Dinelli et al. [J. Chem. Phys. 103 (1995) 10433] is used for energies up to 20000 cm^{-1}, for higher energies the many-body expansion of Sorbie and Murrell is fitted to ab initio calculations [Schinke et al., J. Chem. Phys. 72 (1980) 3909], at large separations long-range terms are combined with accurate diatomic potentials. This produces an accurate global potential which represents all aspects of ground-state H_3^+ including the avoided crossing of the two surfaces and dissociation limits. This surface is suitable for studying spectroscopy, high-lying bound states and reaction dynamics. © 1997 Elsevier Science B.V.

1. Introduction

H_3^+ is the simplest polyatomic molecule. Despite its high symmetry and electronic simplicity the functional form of the potential energy surface (PES) is complicated by the duplicity of dissociation channels, as the charge can reside on either of the fragments, and the low barrier to linearity in the system.

H_3^+ has been the subject of numerous electronic structure calculations [1]. Furthermore, infra-red photodissociation spectroscopy [2,3] has provided information, still poorly understood, about many rovibrational states of H_3^+ near its dissociation limit. As a result of these observations a plethora of fully quantal calculations of increasing sophistication have been performed [4–8] in an attempt to provide a full interpretation. One characteristic of these calculations is that they all used an ab initio surface due to Meyer et al. (MBB) [9] which, though accurate in the near equilibrium region, was not designed to yield the correct behaviour as the molecule dissociates. As has been freely acknowledged [7,10], further progress on this problem cannot be made without an accurate, global PES.

Recent determination of the H_3^+ partition function found that at temperatures above 2000 K estimates of every bound rovibrational states of the molecule are required [11]. This partition function is crucial in determining the behaviour of primordial, so called "metal-free", cool stars. The best available estimate was based on the use of MBB surface and, for reasons discussed below, must constitute an underestimated of the true value.

There are many PESs that cover the low-energy region [12]. The most accurate ab initio PESs have been calculated by Lie and Frye [13] and Röhse et al. [14]. However, these surfaces are valid for exactly the same restricted region as the MBB surface. To

[1] Permanent address: Institute of Applied Physics, Russian Academy of Science, Uljanov Street 46, Nizhnii Novgorod 603024, Russia.

PII S0009-2614(97)00596-4

our knowledge the best published ab initio calculations that give a global coverage are the comparatively old ones by Schinke et al. (SDL) [15].

Recently, Dinelli et al. (DPT) [16] determined a surface for H_3^+ using spectroscopic data. Their effective potential is expressed as a sum of a Born–Oppenheimer (BO) potential and an adiabatic correction. This surface is reliable in a region about the equilateral triangle equilibrium geometry extending as far as the lowest linear geometries, but it gives no information about the dissociation limit for the system.

Surfaces which cover the dissociation region of H_3^+ are much harder to find. To construct a true global PES it is necessary to consider dissociation to both H_2 ($X\ ^1\Sigma_g^+$) + H^+ and H_2^+ ($X\ ^2\Sigma_g^+$) + H($1\ ^2S$) channels. This is because for certain large H_2 / H_2^+ bond lengths H_2^+ + H is actually the lower of the dissociation channels and a full surface necessarily contains an avoided crossing.

There appear to be three global PESs available in the literature. The most accurate is undoubtedly the one given by SDL based on their ab initio calculations. However, this surface is unsatisfactory for a number of reasons: the functional form used has discontinuous derivatives which makes the surface unsuitable for classical trajectory calculations, it does not reflect the symmetry of H_3^+ for much of the surface and the surface also contains unphysically deep minima for certain low-energy geometries. For these reasons this surface, which is not in any case particularly accurate by today's standards, has not been widely used.

More widely used, especially for classical trajectory calculations [17], is the diatoms-in-molecules (DIM) surface of Preston and Tully [18]. Preston and Tully parameterized the two lowest $^1A_1$ to give a PES which is qualitatively correct at all interesting configurations but not particularly accurate, even at low energies. Furthermore the DIM surfaces overestimate the dissociation energy by about 2700 cm^{-1} and does not give the correct long-range behaviour.

Finally, Carter [19] gave an alternative fit to the ab initio data of SDL using a two-surface, Sorbie–Murrell form for the potential [20]. This surface appears never to have been used and, as we discovered, actually gives a very poor fit (for energies above 20000 cm^{-1} the standard deviation is about 6000 cm^{-1}) to the SDL data. Furthermore, the error in the lower dissociation limit is about 2500 cm^{-1} and the representation of the avoided crossing appears to be seriously flawed. According to other studies [21,22] the avoided crossing of the two surfaces occurs at an H_2 distance of $r \simeq 2.5a_0$ and at large H_2 + H^+ separations ($R > 4.0a_0$), since at $R = 4.0a_0$ the splitting is large enough [21] for the system to be considered as diabatic. Carter's surface gives the avoided crossing for a large range of r ($2.5a_0 \lesssim r \lesssim 4.0a_0$) and for values of R below $4.0a_0$.

Thus, the determination of an accurate surface in the dissociation region remains an important problem. The goal of this study is to present a global PES for H_3^+ molecule, which is accurate and covers the whole configuration space up to and above dissociation. Therefore, optimal PESs have been switched by combining the spectroscopic accuracy with the appropriate dissociation limits. At this stage, we have only attempted to determine a Born–Oppenheimer PES for the system.

2. Analytical representation of the PES

As an analytical form of the PES, a combination of two potential forms $V_1(\boldsymbol{R})$ and $V_2(\boldsymbol{R})$ were chosen, using the energy switching approach of Varandas [23]. V_2 reproduces the spectroscopic measurements with quantitative accuracy and is reliable for the region of the minimum of the potential. V_1 should give a realistic representation for configurations with energies higher than those of the spectroscopic data. Furthermore, V_1 should reproduce the correct well depth at the equilibrium geometry. The energy switching (ES) potential is written as

$$V_{ES} = f^+(\Delta E)V_1(\boldsymbol{R}) + f^-(\Delta E)V_2(\boldsymbol{R}), \qquad (1)$$

where $f(\Delta E)$ is the switching function with the general form [23]

$$f^{\pm}(\Delta E) = \frac{1}{2}[1 + \tanh(\pm\gamma\Delta E)] \qquad (2)$$

and

$$\gamma = \gamma_0 + \gamma_1 \Delta E^m, \quad \Delta E = E - E_0. \qquad (3)$$

For H_3^+, E_0 was taken as $\frac{1}{2}(E_d + E_{sp})$, where E_d is the energy at dissociation and E_{sp} is the highest

energy of the region covered by the spectroscopic data, as represented by the V_2 PES. The values of these parameters are given in Table 1. These values give the reference energy, where both $V_1(\boldsymbol{R})$ and $V_2(\boldsymbol{R})$ contribute equally, as $E_0 = 0.13024385\ E_h$ relative to the minimum of the potential.

Following Varandas [23], the optimum value of γ_0 was determined by ensuring that $\tanh(2\gamma_0 \Delta E)$ is within 2% of its asymptotic value at the lowest dissociation limit. Physically m has to be even and was taken equal to 2. In turn, for $m = 2$, γ_1 was chosen by trial and error to optimize the vibrational energies of the molecule ($< 20000\ cm^{-1}$), and the behaviour of the V_{ES} surface at dissociation. Actually, γ should ensure that V_{ES} is totally switched to the V_1 form for energies close to dissociation threshold, which is required for the V_{ES} surface to dissociate correctly.

To define E in Eq. (3) the V_2 form was used, as it is an increasing function of energy. To model the V_2 surface the Born–Oppenheimer potential of Dinelli et al. (DPT) [16] was used. This is expressed as a 7th order polynomial expansion in symmetry coordinates:

$$V_2 = \sum_{n,m,k} V_{n,m,k} S_a^n S_e^{m+k} \cos(k\phi),$$
$$m = 0,2,4,\ldots, \quad k = 0,3,6,\ldots, \tag{4}$$

where $N \geqslant n + m + k$, $N = 7$ and the coefficients of the fit, $V_{n,m,k}$, are given in Table II of DPT [16]. DPT's surfaces reproduce the known spectroscopic data of H_3^+ and its isotopomers to near experimental accuracy. Indeed these surfaces have recently been used to significantly extend assignments for H_3^+ [24]. The accuracy that can be expected for individual isotopomers here is reduced somewhat by our decision to use only the Born–Oppenheimer portion of DPT's surfaces. This decision is justified by the much larger errors inherent in our V_1 surface.

Table 1
Parameters of the V_{ES} potential surface (Eq. (1))

Parameter	Value
E_d / E_h	0.16936100
E_{sp} / E_h	0.09112670
γ_0 / E_h^{-1}	29.3676813
γ_1 / E_h^{-3}	2×10^4
m	2

For the V_1 term the Sorbie–Murrell [20] many-body expansion form was employed. The representation of the PES for H_3^+ is a three-valued surface [20], taking into account all the dissociation schemes. In this approach, the two-body terms are the potential curves of the ground H_2, H_2^+ and the first excited state of H_2^+. The repulsive state of H_2^+ lies above the H + H^+ + H limit, so Carter [19] neglected it. He represented an approximate two-valued surface of H_3^+, by considering two diabatic states V_{aa} and V_{bb}, which correspond to the dissociation channels H_2 + H^+ and H_2^+ + H respectively.

Following Murrell et al. [20], the two-valued representation of the ground and first excited states of H_3^+ are the eigenvalues of the 2×2 matrix. The lowest eigenvalue is given by

$$V_1 = \frac{1}{2}\left[V_{aa} + V_{bb} - \sqrt{(V_{aa} - V_{bb})^2 + V_{ab}^2}\right]. \tag{5}$$

The diabatic surfaces are given by the forms,

$$V_{aa} = V_{HH}^{(2)}(R_1) + V_{HH}^{(2)}(R_2) + V_{HH}^{(2)}(R_3) + V_{aa}^{(3)}(R_1,R_2,R_3), \tag{6}$$

$$V_{bb} = V_{HH^+}^{(2)}(R_1) + V_{HH^+}^{(2)}(R_2) + V_{HH^+}^{(2)}(R_3) + V_{bb}^{(3)}(R_1,R_2,R_3), \tag{7}$$

where R_1, R_2, R_3 are the bond lengths of the three possible diatomic products. $V^{(2)}$ are the two-body terms and $V^{(3)}$ are the three-body terms, which are constructed with full permutation symmetry.

The parameters for the two-body terms were determined using the very high accuracy ab initio data of Bishop and Shih [25] for H_2, and Schwartz and Le Roy [26] for H_2^+. An extended Rydberg functional form for the $V_{HH}^{(2)}$, $V_{HH^+}^{(2)}$ terms was used:

$$V^{(2)} = -D_e\left(1 + \alpha_1 \varrho + \alpha_2 \varrho^2 + \alpha_3 \varrho^3\right)e^{-\alpha_1 \varrho},$$
$$\varrho = R_i - R_e. \tag{8}$$

Parameters and their variances for the $V_{HH}^{(2)}$, $V_{HH^+}^{(2)}$ terms are given in Table 2. For H_2 a total of 87 data points with energies between $-4.7338 \leqslant V^{(2)} \leqslant 23.96$ eV were fitted with standard deviation ~ 0.07 eV and 92 points with energy range $-2.79 \leqslant V^{(2)} \leqslant 25.97$ eV and standard deviation ~ 0.1 eV for H_2^+.

For the short-range (SR) three-body terms, we use the parameters of the 4th order polynomial forms for

Table 2
Parameters of the two-body $V^{(2)}$ terms (Eq. (8)), errors in units of the last decimal places are given in parentheses

Parameter	$V^{(2)}_{HH}$	$V^{(2)}_{HH^+}$
D_e /eV	4.73379 [25]	2.79282 [26]
R_e /Å	0.74080 [25]	1.05835 [26]
α_1 /Å^{-1}	4.38127(46)	3.09142(77)
α_2 /Å^{-2}	6.12491(844)	3.43864(478)
α_3 /Å^{-3}	5.99582(606)	2.70834(167)

$V^{(3)SR}_{bb}$ and $V^{(3)}_{ab}$, obtained by Carter [19]. The validity and the physical behaviour of these terms was examined and found to be satisfactory. The more important $V^{(3)SR}_{aa}$ term is represented as a 7th order polynomial given by

$$V^{(3)SR} = P(R_1,R_2,R_3)T(R_1,R_2,R_3), \tag{9}$$

$$\begin{aligned} P(R_1,R_2,R_3) &= V_0\Bigg(1 + \sum_{i=1}^{3} C_i \rho_i + \sum_{i\leqslant j}^{3} C_{ij}\rho_i\rho_j \\ &+ \sum_{i\leqslant j\leqslant k}^{3} C_{ijk}\rho_i\rho_j\rho_k \\ &+ \sum_{i\leqslant j\leqslant k\leqslant l}^{3} C_{ijkl}\rho_i\rho_j\rho_k\rho_l \\ &+ \sum_{i\leqslant j\leqslant k\leqslant l\leqslant n}^{3} C_{ijkln}\rho_i\rho_j\rho_k\rho_l\rho_n \\ &+ \sum_{i\leqslant j\leqslant k\leqslant l\leqslant n\leqslant m}^{3} C_{ijklnm}\rho_i\rho_j\rho_k\rho_l\rho_n\rho_m \\ &+ \sum_{i\leqslant j\leqslant k\leqslant l\leqslant n\leqslant m\leqslant z}^{3} C_{ijklnmz}\rho_i\rho_j\rho_k\rho_l\rho_n\rho_m\rho_z\Bigg), \end{aligned} \tag{10}$$

$$T(R_1,R_2,R_3) = \prod_{i=1}^{3}\left[1 - \tanh\left(\tfrac{1}{2}g_i\rho_i\right)\right],$$

$$\rho = R_i - R_0, \quad i = 1,2,3. \tag{11}$$

The parameters in this form were determined by a non-linear least-square fitting of the lower surface, Eq. (5), to the ab initio data of Schinke et al. [15].

SDL's data are confined to 650 grid points with boundaries $0.0a_0 \leqslant R \leqslant 10.0a_0$, $0.6a_0 \leqslant r \leqslant 2.6a_0$ and $0° \leqslant \theta \leqslant 90°$ in Jacobi coordinates. In these coordinates, r is the H–H distance, R is the distance between H^+ and the center of mass of H_2, and θ is the angle $(\boldsymbol{r}, \boldsymbol{R})$.

A number of ways of fitting these data was tested. In our final fits 327 $V_l(r,R,\theta)$ geometries were used. These are all the points for which 20000 cm^{-1} $< V_l <$ 70000 cm^{-1} and $r < 2.6a_0$, since configurations with $r \geqslant 2.5a_0$ and large $R \geqslant 4.0a_0$ (30 points in total) are described by the V_{bb} diabatic surface [15], due to the avoided crossing.

For fitting the sophisticated interactive non-linear least squares (I-NoLLS) [27] program was used. The singular value decomposition (SVD) method was used for modelling the data and selecting the parameter scalings according to their estimated uncertainty, such as their 95% confidence limit [27,28]. To improve the conditioning of the least-squares fit the Levenberg–Marquardt algorithm was employed to select the step size in the parameter space. Initially, we set the parameter step large enough, compared with the largest singular value of the Jacobian matrix, to ensure that the first step is along the direction of the steepest descent and we continued to decrease it, if it resulted in a reduction in the sum of squares, to convergence.

Finally, 32 parameters were determined for $V^{(3)SR}_{aa}$, using the 327 data points. The standard deviations achieved after the fit are $\sim$ 280 cm^{-1} for the V_1 form and globally $\sim$ 252 cm^{-1} for the V_{ES}. If the 30 extra points in the above energy regime with $r = 2.6a_0$ and $R \geqslant 4.0a_0$ are included, then the standard deviations are $\sim$317 cm^{-1} for the V_1 and $\sim$301 cm^{-1} for the V_{ES}. The major source of increase in the standard deviations comes from points with linear configurations, as the separation between the two surfaces is smaller than for equilateral geometries. These configurations are represented much better by the V_{ES} form.

Table 3 reports the parameters of the three-body terms $V^{(3)SR}_{aa}$, $V^{(3)SR}_{bb}$ and $V^{(3)}_{ab}$ for the V_1 potential energy surface. The values of the calculated parameters for the $V^{(3)SR}_{aa}$ term are tabulated together with their variances (squared uncertainties). Furthermore, the parameter correlation was verified. The largest value is $-$ 0.9675 for the correlation between the $C_{1111112}$ and $C_{1111222}$ parameters.

The functional form used to represent the three-body terms does not display the correct behaviour

Table 3
Parameters of the three-body terms of the two-valued H_3^+ potential (Eq. (5)), errors in units of the last decimal places are given in parentheses

Parameter	$V_{aa}^{(3)SR}$	$V_{bb}^{(3)SR}$ [19]	$V_{ab}^{(3)}$ [19]
C_1 /Å^{-1}	−0.487635(40)	0.0393	0.3192
C_{11} /Å^{-2}	0.460931(115)	−0.0035	−0.7084
C_{12}	−1.093472(360)	0.0711	−0.2253
C_{111} /Å^{-3}	0.113334(639)	0.0269	0.9527
C_{112}	−0.170666(492)	0.0078	0.1778
C_{123}	1.043245(2940)	0.1452	0.0597
C_{1111} /Å^{-4}	−0.137693(1630)	0.0097	−0.5182
C_{1112}	0.586113(4600)	−0.0318	−0.1000
C_{1122}	−0.678741(6780)	0.0234	0.1582
C_{1123}	−0.242872(2230)	0.0305	0.0426
C_{11111} /Å^{-5}	0.028827(1400)	–	–
C_{11112}	−0.249638(5520)	–	–
C_{11122}	0.212290(2070)	–	–
C_{11123}	−0.257605(15300)	–	–
C_{11223}	0.235806(20500)	–	–
C_{111111} /Å^{-6}	0.082524(467)	–	–
C_{111112}	−0.247365(2540)	–	–
C_{111122}	0.414443(5860)	–	–
C_{111222}	−0.518085(11400)	–	–
C_{111123}	0.622019(20400)	–	–
C_{111233}	−0.216965(10600)	–	–
C_{112233}	−0.890872(36200)	–	–
$C_{1111111}$ /Å^{-7}	−0.044282(32)	–	–
$C_{1111122}$	−0.221662(941)	–	–
$C_{1111112}$	0.159334(341)	–	–
$C_{1111123}$	−0.377969(2260)	–	–
$C_{1111222}$	0.108116(329)	–	–
$C_{1111223}$	0.240714(1640)	–	–
$C_{1112223}$	−0.085919(3380)	–	–
$C_{1122333}$	0.032833(1900)	–	–
V_0 /eV	3.782643(4)	10.2785	0.3878
R_0 /Å	0.891756	1.5358	1.1783
g_1 /Å^{-1}	0.820040(3)	1.5027	2.1492

when one atom/ion is well separated from the other two. To describe the charge-induced dipole and charge-quadrupole contributions we introduced long-range (LR) values known from perturbation theory [22]. For large $H^+ + H_2$ separations the analytical form for the V_{aa}^{LR} term is defined [22] by

$$V_{aa}^{LR} = \frac{[A_0(r) + A_2(r)P_2(\cos\theta)]}{R^4} + \frac{Q_2(r)P_2(\cos\theta)}{R^3}, \quad (12)$$

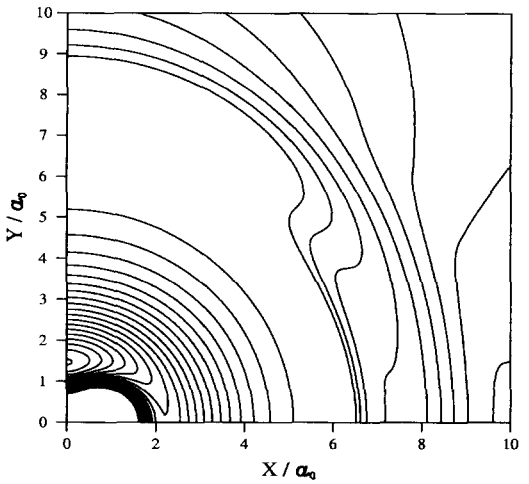

Fig. 1. Contours of the H_3^+ potential energy surface, V_{ES} (Eq. (1)), for H^+ moving around H–H with a fixed H–H bond length at 0.74 Å. The equipotential curves are drawn from 1850 to 35150 cm^{-1} at increments of 1850 cm^{-1}, and from 37000 to 37190 cm^{-1} with intervals of 27 cm^{-1} to emphasize the dissociation region.

where the functional forms of A_0, A_2, Q_2 are given in Ref. [22], and P_2 are the Legendre polynomials. We modified the three-body term using a switching function based on the Jacobi coordinates, R, which

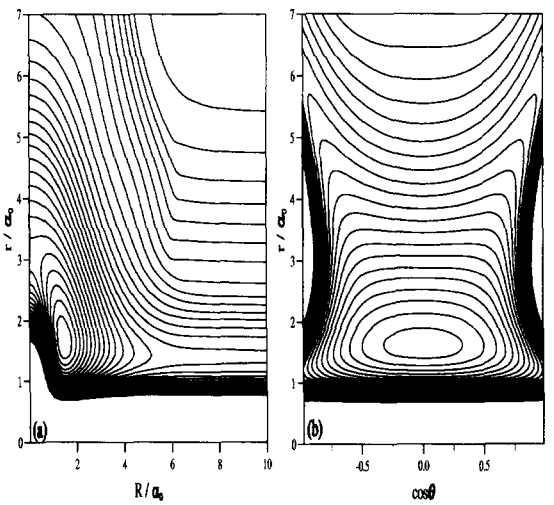

Fig. 2. Contours of the H_3^+ potential energy surface, V_{ES} (Eq. (1)), for (a) $\theta = 90°$, and (b) $R = 1.65a_0$. Contour intervals are of 2500 cm^{-1} and for energies from 2500 to 75000 cm^{-1}.

give the $H^+ + H_2$ separation. The revised three-body term, $V_{aa}^{(3)}$, is given by

$$V_{aa}^{(3)} = g(R)V_{aa}^{(3)SR} + [1 - g(R)]V_{aa}^{LR} \quad (13)$$

with the switching function defined by

$$g(R) = \begin{cases} 1 & R < R_{LIM}, \\ \cos^2\left[\dfrac{\pi(R - R_{LIM})}{2(R_M - R_{LIM})}\right] & R_{LIM} \leqslant R \leqslant R_M, \\ 0 & R > R_M, \end{cases} \quad (14)$$

where $R_{LIM} = 4.0a_0$ and $R_M = 10.0a_0$, as this is the end of SDL's grid. The value of the R_{LIM} was chosen by trial and error to both decrease the standard deviations for the V_{ES} form to the SDL data and to match smoothly onto the $V_{aa}^{(3)SR}$ term.

For the upper diabatic state the $V_{bb}^{(3)}$ term has the form

$$V_{bb}^{(3)} = g(r)V_{bb}^{(3)SR} + [1 - g(r)]V_{bb}^{LR}, \quad (15)$$

where the V_{bb}^{LR} is defined [29] by

$$V_{bb}^{LR} = -\frac{d_1}{r^4} - \frac{d_2}{r^6} \quad (16)$$

and is the term for large $H_2^+ + H$ distances, with H atom dipole polarizability of $d_1 = 4.5$ au and quadrupole polarizability of $d_2 = 15.0$ au [29]. For the switching function $g(r)$ we use Eq. (14) with $r_{LIM} = 5.0a_0$ and $r_M = 11.0a_0$.

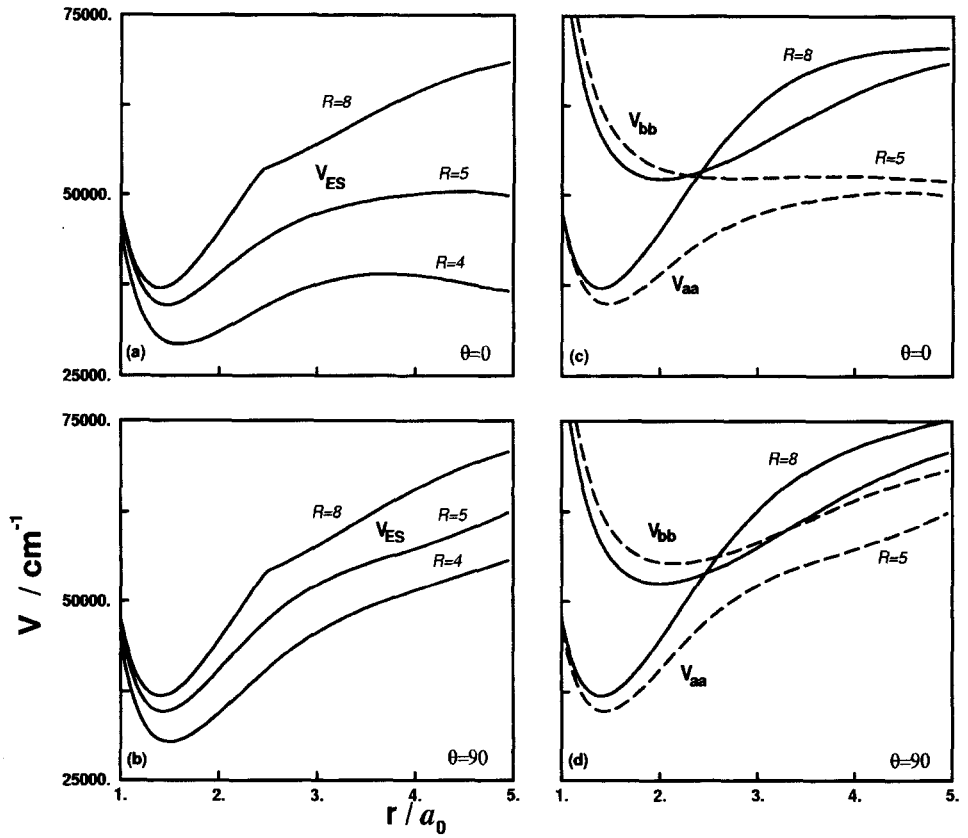

Fig. 3. (a,b) Potential curves for the V_{ES} (Eq. (1)) for $R = 4.0$, 5.0 and $8.0a_0$ and for $\theta = 0°$ and 90° respectively. The avoided crossing occurs for $r \sim 2.5a_0$ and for $R \gtrsim 8.0a_0$. (c,d) Potential curves for the V_{aa}, V_{bb} diabatic surfaces of H_3^+. Full lines (—) are for $R = 8.0a_0$ and dashed lines (- - -) for $R = 5.0a_0$. The dependence of θ is shown, for linear configurations the separation between the two states is smaller.

To assess our potential, we compared the dissociation limits with those given in Table XI of Röhse et al. [14]. Our energy for dissociation into $H_2 + H^+$ is 37193 cm^{-1}, just 23 cm^{-1} higher than the very accurate Born–Oppenheimer value. The next dissociation limit for H^+ and an elongated H_2 is 54386 cm^{-1}, 460 cm^{-1} higher than the best estimated limit. Our barrier to linearization lies at 14260 cm^{-1}, which is underestimated by 39 cm^{-1}. Finally, there is an error of ~ 150 cm^{-1} for the $H + H + H^+$ dissociation energy.

Table 4
Comparison of selected H_3^+ vibrational term values, in cm^{-1}, computed with V_{ES} and BO-DPT [16] potential surfaces. For both surfaces the ground state is at energy 4362.78 cm^{-1}

State No.	ES	(ES-DPT)
1	2521.00	0.01
2	3178.76	0.00
3	4777.16	0.03
8	7283.27	0.06
9	7766.89	0.04
11	8485.50	0.03
12	8995.66	0.12
13	9107.50	0.11
18	10586.40	0.05
19	10639.32	0.06
21	10911.30	0.14
22	11315.12	0.06
23	11647.54	0.11
28	12358.72	0.12
29	12459.74	0.05
31	12682.01	0.04
32	13271.97	0.02
33	13303.24	0.14
38	13699.46	0.17
39	14037.99	0.28
41	14197.94	−0.01
42	14451.01	−0.02
43	14644.46	0.04
48	15050.46	0.26
49	15095.33	0.25
51	15184.37	−0.13
52	15306.18	−0.27
53	15753.07	−0.19
58	16178.66	0.27
59	16225.72	0.11
61	16420.67	−0.26
62	16524.44	−0.67
63	16643.29	0.81
68	17027.71	−0.35
69	17186.39	−0.67

Figs. 1 and 3 represent views of the V_{ES} (Eq. (1)) potential surface. In Fig. 1 equipotential curves are shown for H^+ moving around of an H_2 molecule. Fig. 2 shows contours of the potential surface in (R,r)-plane for fixed $\theta = 90°$, and (θ,r)-plane for fixed $R = 1.65a_0$.

In Fig. 3 we represent the V_{ES} surface for several values of R and θ, as well as the diabatic V_{aa}, V_{bb} states. The avoided crossing occurs at $r \simeq 2.5a_0$, as we can see in Fig. 3(a,b), and for large values of R, $R \geqslant 8.0a_0$. The plots of the diabatic states are shown in Fig. 3(c,d) for the region of the avoided crossing. As shown previously by Preston and Tully [18], the splitting of the two surfaces is smaller for linear configurations than for equilateral configurations. This behaviour is demonstrated by V_{ES} form as it is shown in Fig. 3(c,d). The region of the avoided crossing appears to be qualitatively well described.

Finally, we calculated vibrational levels to about 20000 cm^{-1} above the minimum using our newly constructed, V_{ES}, potential and the BO-DPT surface of Dinelli et al. [16]. In these calculations we used atomic masses of 1.0076422 a.m.u. (mass of hydrogen atom minus one third of an electron) and parameters as presented by Neale et al. [30]. These agree to better than 1 cm^{-1} (see in Table 4), with those calculated using the BO-DPT surface. This demonstrates that the accuracy of the spectroscopically determined surface has been retained. The current surface serves to correct the high energy and asymptotic behaviour of the BO-DPT potential and, as is clear, these corrections have almost no influence on the calculated vibrational energies, although they will obviously be critical near dissociation.

3. Discussion and conclusions

In this Letter we present a new, two-valued, global H_3^+ potential energy surface. This surface is constructed by combining the best information available for each region of the surface. At lower energies experimental data, in the form of a spectroscopically determined Born–Oppenheimer surface [16] is used. At intermediate energies we present a new fit to the best available ab initio data [15]. For dissociating channels we employ long-range interaction terms

determined by perturbation theory [22]. Therefore, our potential gives both the accuracy of the spectroscopic observations with the appropriate dissociation limits. All the interesting configurations, such as dissociation limits, barriers, as well as the region of the avoided crossing, are satisfactorily reproduced. The major limitation is the ab initio data used to fit at higher energies. Thus, this surface will provide a suitable form for reparameterization as new experimental or high level ab initio data becomes available.

Finally, it should be noted that inclusion of the correct long-range behaviour into over surfaces means that our surface is considerably more attractive at long range than previous global ones. Among other things, this means that our surface will support considerably more vibrationally bound states than those found by studies on more limited surfaces [4–8,31]. These states are likely to be harder to represent as they will require considerably more extensive grids. Extra states will undoubtedly lead to an increase in the partition function for H_3^+.

A FORTRAN code for the V_{ES} potential energy surface is available via either our group World Wide Web page on www.tampa.phys.ucl.ac.uk or anonymous ftp from IP address 128.40.2.160 (jonny.phys.ucl.ac.uk) in the file pub/vr/potentials/H3p.VES.f.

Acknowledgements

R.P. gratefully acknowledges a TMR Fellowship, under contract ERBFMBICT 960901; this work was also supported by the UK Engineering and Physical Sciences Research Council. The work of O.L.P. was partially supported by the Russian Fund for Fundamental Studies.

References

[1] J.B. Anderson, J. Chem. Phys. 96 (1992) 3702 (see Table 1).
[2] A. Carrington, R.A. Kennedy, J. Chem. Phys. 81 (1984) 91.
[3] A. Carrington, I.R. McNab, Y.D. West, J. Chem. Phys. 98 (1993) 1073.
[4] J.R. Henderson, J. Tennyson, Chem. Phys. Lett. 173 (1990) 133.
[5] J.R. Henderson, J. Tennyson, B.T. Sutcliffe, J. Chem. Phys. 96 (1992) 2426.
[6] M.J. Bramley, J.W. Tromp, T. Carrington Jr, G.C. Corey, J. Chem. Phys. 100 (1994) 6175.
[7] J.R. Henderson, J. Tennyson, Mol. Phys. 89 (1996) 953.
[8] V.A. Mandelshtam, H.S. Taylor, J. Chem. Soc., Far. Trans. 93 (1997) 847.
[9] W. Meyer, P. Botschwina, P. Burton, J. Chem. Phys. 84 (1986) 891.
[10] J. Tennyson, B.M. Dinelli, O.L. Polyansky, J. Mol. Struct. (Theochem) 341 (1995) 133.
[11] L. Neale, J. Tennyson, Astrophys. J. 454 (1995) L169.
[12] J. Tennyson, Rep. Prog. Phys. 57 (1995) 421.
[13] G.C. Lie, D. Frye, J. Chem. Phys. 96 (1992) 6784.
[14] R. Röhse, W. Kutzelning, R. Jaquet, W. Klopper, J. Chem. Phys. 101 (1994) 2231.
[15] R. Schinke, M. Dupuis, W.A. Lester Jr., J. Chem. Phys. 72 (1980) 3909.
[16] B.M. Dinelli, O.L. Polyansky, J. Tennyson, J. Chem. Phys. 103 (1995) 10433.
[17] J.M. Gomez Llorente, E. Pollak, J. Chem. Phys. 89 (1988) 1195.
[18] R.K. Preston, J.C. Tully, J. Chem. Phys. 54 (1971) 4297.
[19] S. Carter, unpublished results (see Ref. [20], Chapter 11).
[20] J.N. Murrell, S. Carter, S.C. Farantos, P. Huxley, A.J.C. Varandas, Molecular potential energy functions (Wiley, New York, 1984).
[21] C.W. Bauschlicher Jr., S.V. O'Neil, R.K. Preston, H.F. Schaefer III, C.F. Bender, J. Chem. Phys. 59 (1973) 1286.
[22] C.F. Giese, W.R. Gentry, Phys. Rev. A 10 (1974) 2156.
[23] A.J.C. Varandas, J. Chem. Phys. 105 (1996) 3524.
[24] B.M. Dinelli, L. Neale, O.L. Polyansky, J. Tennyson, J. Mol. Spect. 181 (1997) 142.
[25] D.M. Bishop, S.-K. Shih, J. Chem. Phys. 64 (1976) 162.
[26] C. Schwartz, R.J. Le Roy, J. Mol. Spectr. 121 (1987) 420.
[27] M.M. Law, J.M. Hutson, Comput. Phys. Commun., in press (1997).
[28] W.H. Press, B.P. Flannery, S.A. Teukolsky, W.T. Vetterling, Numerical recipes (Cambridge Univ. Press, Cambridge, (1986).
[29] B.H. Bransden, Atomic collision theory (Benjamin, New York, 1970).
[30] L. Neale, S. Miller, J. Tennyson, Astrophys. J. 464 (1996) 516.
[31] M. Berblinger, C. Schlier, J. Tennyson, S. Miller, J. Chem. Phys. 96 (1992) 6842.